The Astrophysical Journal, 995:138 (8pp), 2025 December 20 https://doi.org/10.3847/1538-4357/ae1ef3
© 2025. The Author(s). Published by the American Astronomical Society.
OPEN ACCESS

Magnetized Accretion Flows: The Key Roles of Viscosity and Black Hole Mass

Wen-Biao Wu
College of Physics and Electronic Information, Nanchang Normal University, Nanchang 330032, People's Republic of China; wuwenbiao89@ncnu.edu.cn
Received 2025 October 19; revised 2025 November 7; accepted 2025 November 10; published 2025 December 11

Abstract

In our previous work, we constructed a black hole accretion model incorporating magnetic fields and disk winds. However, this model was derived under conditions of a small viscosity parameter α ($\alpha < \alpha_{\rm crit}$, where $\alpha_{\rm crit}$ is the critical viscosity parameter) and for accretion systems around stellar-mass black holes. In the present study, we extend this model to regimes with $\alpha > \alpha_{\rm crit}$ and to supermassive black hole accretion systems. Our study reveals that under the condition of $\alpha > \alpha_{\rm crit}$, the topological structure of thermal equilibrium solutions in black hole accretion disks undergoes significant changes. In the saturated state, the region dominated by advective cooling is confined to the inner disk, yet it expands radially as α increases. This may provide a theoretical explanation for the strong advection-dominated accretion flow (ADAF) principle, specifically addressing the connection problem between the standard thin disk (SSD) and ADAF. Furthermore, we find that the properties of the accretion disk depend on the mass of the central black hole. For stellar-mass black hole accretion systems, the optically thick radiative cooling solutions (similar to the SSD) remain stable, whereas for black holes with $M \geqslant 10^5 M_{\odot}$, the optically thick radiative cooling solutions exhibit unstable behavior. These differences may help explain the distinct variability behaviors observed between X-ray binaries and active galactic nuclei.

Unified Astronomy Thesaurus concepts: High energy astrophysics (739); Black holes (162); Magnetic fields (994); Accretion (14)

1. Introduction

Accretion disks serve as the central engines for various high-energy astrophysical phenomena in the Universe, such as black hole X-ray binaries (XRBs) and active galactic nuclei (AGNs; e.g., S. Kato et al. 2008). The earliest analytical model describing black hole accretion was the standard thin disk (SSD) model proposed by N. I. Shakura & R. A. Sunyaev (1973), which is characterized by efficient radiative cooling of locally generated viscous heat, resulting in a geometrically thin disk. Subsequently, to explain the observed hard spectra, the optically thin, two-temperature Shapiro–Lightman–Eardley (SLE) model was proposed (S. L. Shapiro et al. 1976). However, this model was thermally unstable and was eventually replaced by the optically thin, advection-dominated accretion flow (ADAF; R. Narayan & I. Yi 1994, 1995). When the accretion rate approaches or exceeds the Eddington accretion rate, the accretion mode transitions to a slim disk, where optically thick advective dominance leads to photon trapping (M. A. Abramowicz et al. 1988).

The models discussed above largely fail to account for the effects of outflows. Pioneering research by Shakura and Sunyaev on the SSD model revealed that when the accretion rate approaches or exceeds the Eddington limit, the radiative force overwhelms the gravitational force, suggesting that outflows may be inevitable (N. I. Shakura & R. A. Sunyaev 1973). Subsequently, T. Piran (1978) investigated the influence of disk winds on the stability of the SSD model, and M. A. Abramowicz (1981) conducted similar stability analyses. In the article establishing the ADAF model, R. Narayan & I. Yi (1994) found that their solution featured a positive Bernoulli parameter, indicating the potential for outflows or jets. Later, theoretical studies suggested that such outflows are inevitable (e.g., W.-M. Gu & J.-F. Lu 2007; W.-M. Gu 2015; X. Cao & W.-M. Gu 2015, 2022; J. Feng et al. 2019). The most renowned analytical work explaining outflows is that of R. D. Blandford & M. C. Begelman (1999), who proposed a scenario in which the accretion rate varies as a function of radius. Based on this assumption, extensive research has been conducted to study the structure and properties of accretion disks that incorporate outflows (e.g., W.-B. Wu et al. 2022; J. Huang et al. 2023). Furthermore, numerical simulations have confirmed the existence of outflows in various accretion systems, such as geometrically thin disks (e.g., K. Ohsuga & S. Mineshige 2011; M. Nomura et al. 2016, 2020), super-Eddington accretion disks (e.g., K. Ohsuga et al. 2005; K. Ohsuga & S. Mineshige 2011; Y.-F. Jiang et al. 2014; A. Sadowski et al. 2014; A. Sadowski & R. Narayan 2015; T. Kitaki et al. 2017, 2018; F. Zahra Zeraatgari et al. 2020; J. Huang et al. 2023), and radiatively inefficient accretion flows (e.g., J. M. Stone et al. 1999; R. Narayan et al. 2012; F. Yuan et al. 2012a, 2015; F. Yuan et al. 2012b). Additionally, accumulating observational evidence indicates that outflows are ubiquitous in accreting compact objects, including black hole XRBs (e.g., J. Homan et al. 2016), the Galactic Center (e.g., Q. D. Wang et al. 2013; R.-Y. Ma et al. 2019), and low-luminosity AGNs (e.g., J. Park et al. 2019; F. Shi et al. 2021).

It is now widely accepted that angular momentum transfer in accretion disks is governed by the magnetorotational instability (MRI; S. A. Balbus & J. F. Hawley 1991). Consequently, magnetic fields play a critical role in determining the properties of accretion disks; for instance, they can suppress disk instabilities (e.g., M. C. Begelman & J. E. Pringle 2007; H. Oda et al. 2009; S.-M. Zheng et al. 2011; X.-F. Yu et al. 2015; A. Habibi & S. Abbassi 2019) and drive outflows (e.g., X. Cao & H. C. Spruit 2013; J. Jacquemin-Ide et al. 2019) or jets (R. D. Blandford & D. G. Payne 1982). Numerical studies further reveal that magnetic field geometry—whether purely toroidal or purely poloidal—can lead to marked differences in

Original content from this work may be used under the terms of the Creative Commons Attribution 4.0 licence. Any further distribution of this work must maintain attribution to the author(s) and the title of the work, journal citation and DOI.

the morphology and dynamics of radiatively inefficient accretion flows (e.g., I. V. Igumenshchev et al. 2003). Moreover, strongly magnetized disks offer a compelling explanation for phenomena such as state transitions in XRBs (e.g., M. C. Begelman et al. 2015), hysteresis (e.g., N. Scepi et al. 2024; J. Huang et al. 2025), and the timescales associated with changing-look AGNs (e.g., J. Dexter & M. C. Begelman 2019; J. Feng et al. 2021; N. Scepi et al. 2021; W.-B. Wu & W.-M. Gu 2023). These crucial roles of magnetic fields have been extensively confirmed by numerical simulations (e.g., A. Sadowski 2016; G. Salvesen et al. 2016; J. Huang et al. 2023; N. Scepi et al. 2024).

Recently, we developed an accretion model that incorporates magnetic pressure and disk winds based on numerical simulations (J. Huang et al. 2023). This model shows that saturated magnetic pressure can significantly alter the properties of accretion disks. However, it was solved under the conditions of a small viscosity parameter α ($\alpha < \alpha_{\rm crit}$, where $\alpha_{\rm crit}$ is the critical viscosity parameter) and for stellar-mass black hole systems. In traditional accretion theory, X. Chen et al. (1995) found that accretion disk thermal equilibrium solutions exhibit a novel topological structure at $\alpha > \alpha_{\rm crit}$. Furthermore, both theoretical (e.g., N. I. Shakura & R. A. Sunyaev 1973) and numerical studies (e.g., Y.-F. Jiang et al. 2019) have revealed that radiation pressure plays a significantly more important role in accretion disks around supermassive black holes compared to stellar-mass black holes, which may lead to properties distinct from those in stellar-mass black hole systems. Motivated by the above considerations, we have revisited the thermal equilibrium solutions of black hole accretion disks. This paper is organized as follows: Section 2 presents the basic equations of the model; Section 3 describes the numerical results and analysis; and Section 4 provides a summary and discussion.

2. Basic Equations

This section outlines the fundamental equations of our model. We consider a steady, axisymmetric accretion flow under the pseudo-Newtonian potential $\Phi = -GM_{\rm BH}/(R - R_g)$ (B. Paczyński & P. J. Wiita 1980), where $M_{\rm BH}$ denotes the black hole mass and R_g is the Schwarzschild radius. The vertical scale height of the flow is given by $H = c_s/\Omega_K$, in which Ω_K represents the Keplerian angular velocity, and $c_s = (P/\rho)^{1/2}$ is the sound speed, with P and ρ being the pressure and mass density, respectively. The kinematic viscosity coefficient is prescribed via the standard α-viscosity ansatz: $\nu = \alpha c_s H$, where α is the constant viscosity parameter.

In this work, the effects of strong magnetic fields are considered. Therefore, the equation of state takes the form

$$P = P_{\rm gas} + P_{\rm rad} + P_m, \tag{1}$$

where $P_{\rm gas}$ denotes the gas pressure, $P_{\rm rad}$ denotes the radiation pressure, and P_m denotes the magnetic pressure. These components are defined as follows:

$$P_{\rm gas} = \frac{\rho k_B}{\mu m_p}(T_i + T_e), \tag{2}$$

$$P_{\rm rad} = \frac{Q_{\rm rad}}{4c}\left(\tau + \frac{2}{\sqrt{3}}\right), \tag{3}$$

$$P_m = \frac{B^2}{8\pi}, \tag{4}$$

where B is the magnetic field strength, and T_i and T_e represent the ion temperature and the electron temperature, respectively, with $T_e = \min\ (T_i, 6 \times 10^9\ {\rm K})$. The mean molecular weight is taken as $\mu = 0.617$. The total optical depth is defined as $\tau = (\kappa_{\rm es} + \kappa_{\rm abs})\rho H$, where $\kappa_{\rm es} = 0.34 {\rm cm^2\ g^{-1}}$ and $\kappa_{\rm abs} = 0.27 \times 10^{25} \rho T_e^{-3.5}\ \ {\rm cm^2\ g^{-1}}$ (e.g., M. A. Abramowicz et al. 1996).

According to M. C. Begelman & J. E. Pringle (2007), the MRI drives a dynamo that amplifies the toroidal magnetic field until it saturates. The saturation level is determined by the Alfvén speed V_A ($\equiv\sqrt{P_m/\rho}$), which is approximately equal to the geometric mean of the Keplerian velocity V_K and the gas sound speed $c_g = \sqrt{P_{\rm gas}/\rho}$ (M. E. Pessah & D. Psaltis 2005):

$$V_A^2 = \xi V_K c_g, \tag{5}$$

where we introduced a dimensionless parameter ξ to represent the relative contribution of magnetic pressure to the total pressure, constrained to [0, 1].

The basic equations governing the flow consist of the continuity, radial momentum, azimuthal momentum, and energy equations. The continuity equation takes the form:

$$\frac{1}{R}\frac{d}{dR}(R\Sigma V_R) + \frac{1}{2\pi R}\frac{d\dot{M}_w}{dR} = 0, \tag{6}$$

where Σ is the surface density, defined as $\Sigma \equiv 2\rho H$, and V_R is the radial velocity, which is defined to be negative when the flow is inward. The outflow mass-loss rate $\dot{M}_w$ is (C. Knigge 1999)

$$\dot{M}_w(R) = \int_{R_{\rm in}}^{R} 4\pi R' \dot{m}_{\rm w}(R') dR', \tag{7}$$

where $R_{\rm in}$ represents the radius at the inner edge of the disk and $\dot{m}_w$ denotes the mass-loss rate per unit area from each face of the disk.

The influence of outflows motivates our assumption that the accretion rate $\dot{M}$ varies radially according to (R. D. Blandford & M. C. Begelman 1999)

$$\dot{M} = -2\pi R\Sigma V_R = \dot{M}_{\rm outer}\left(\frac{R}{R_{\rm outer}}\right)^p, \tag{8}$$

where $\dot{M}_{\rm outer}$ denotes the mass accretion rate at the outer boundary $R_{\rm outer}$. In this work, we follow the assumption by W.-B. Wu et al. (2022) that p is proportional to the disk thickness: $p = \lambda(H/R)$, where λ is a dimensionless parameter.

Using Equations (6)–(8), we derive the following relation:

$$\dot{m}_w = \frac{\dot{M}p}{4\pi R^2}. \tag{9}$$

The integrated radial momentum equation and the azimuthal equation of motion can be, respectively, written as

$$V_R\frac{dV_R}{dR} + \left(\Omega_K^2 - \Omega^2\right)R + \frac{1}{\rho}\frac{dP}{dR} = 0, \tag{10}$$

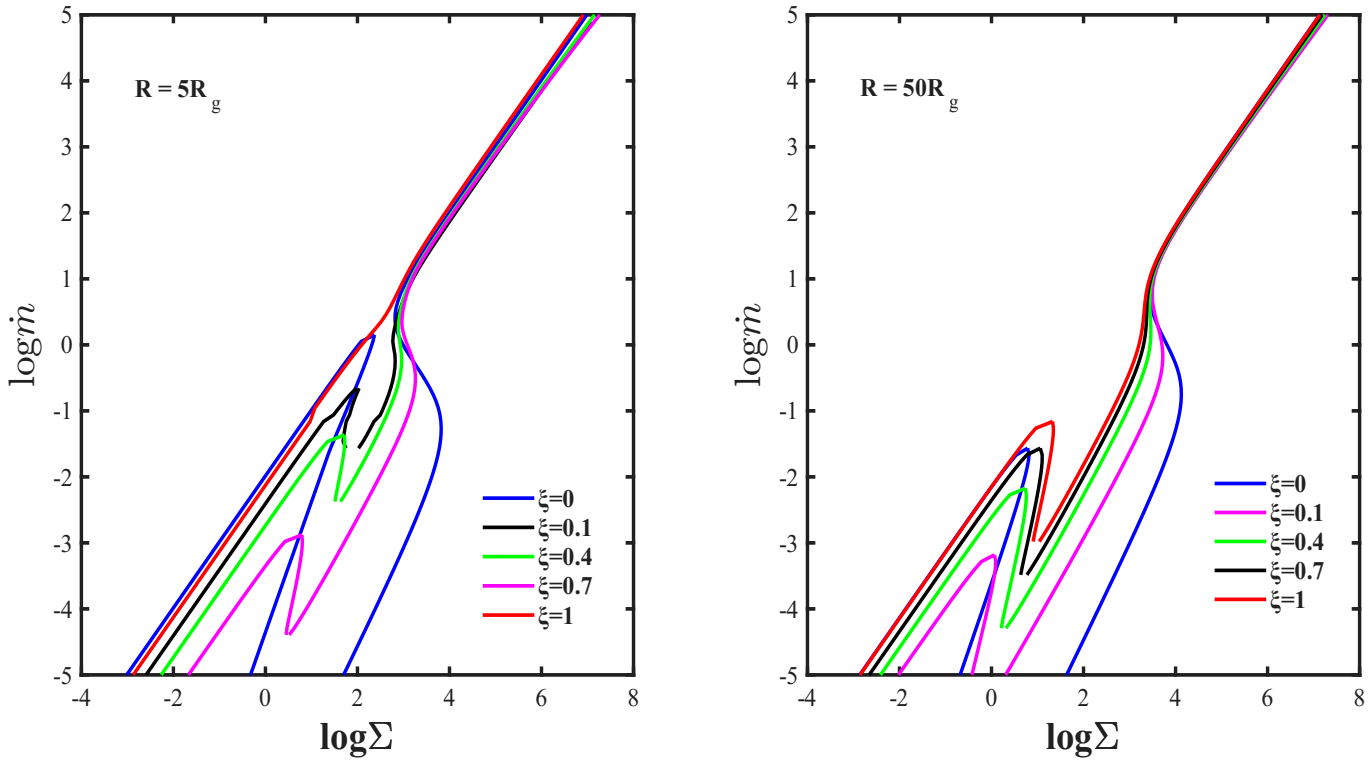

Figure 1. The thermal equilibrium solution for an accretion disk with $M_{\rm BH} = 10M_{\odot}$ and $\alpha = 0.1$ is shown in the figure. This figure reveals the influence of the magnetic field strength on the disk's topological structure.

$$-\frac{1}{R}\frac{d}{dR}(R^3\Sigma V_R\Omega) + \frac{1}{R}\frac{d}{dR}\left(R^3\nu\Sigma\frac{d\Omega}{dR}\right) - \frac{(lR)^2\Omega}{2\pi R}\frac{d\dot{M}_w}{dR} = 0, \tag{11}$$

where the final term on the left-hand side of Equation (11) represents the angular momentum carried by the outflow. Here, the parameter l defines the outflow's angular momentum: $l = 0$ corresponds to a nonrotating outflow; $l = 1$ indicates that the outflow carries the specific angular momentum of its ejection point; and $l > 1$ describes centrifugally driven magnetic disk winds that extract additional angular momentum from the disk (C. Knigge 1999).

The energy balance in the accretion disk is governed by the equation:

$$Q_{\rm vis} = Q_{\rm adv} + Q_{\rm rad} + Q_{\rm w}, \tag{12}$$

where $Q_{\rm vis}$ denotes the viscous heating rate, $Q_{\rm adv}$ denotes the advective cooling rate, and $Q_{\rm rad}$ denotes the radiative cooling rate. These terms are defined as follows:

$$Q_{\rm vis} = \nu\Sigma\left(R\frac{d\Omega}{dR}\right)^2, \tag{13}$$

$$Q_{\rm adv} = \Sigma V_R T\frac{ds}{dR} = \Sigma V_R\left(\frac{1}{\gamma-1}\frac{dc_s^2}{dR} - \frac{c_s^2}{\rho}\frac{d\rho}{dR}\right), \tag{14}$$

$$Q_{\rm rad} = 8\sigma T_e^4\left(\frac{3\tau}{2} + \sqrt{3} + \frac{8\sigma T_e^4}{Q_{\rm br}^-}\right)^{-1}, \tag{15}$$

Equation (15) is valid in both optically thin and optically thick regimes (R. Narayan & I. Yi 1995). The bremsstrahlung cooling is given by (e.g., M. A. Abramowicz et al. 1995)

$$Q_{\rm br}^- = 1.24\times10^{21}H\rho^2T_e^{1/2}\ {\rm erg\ s^{-1}\ cm^{-2}}. \tag{16}$$

The term Q_w in Equation (12) represents the energy carried away by outflows, and is given by

$$Q_w = 2f\eta\dot{m}_w V_K^2, \tag{17}$$

where the factor 2 accounts for the outflow energy emitted from both sides of the accretion disk. Here, η is an energy parameter characterizing the outflow.

By using Equation (6) and integrating Equation (11), we obtain

$$\nu\Sigma = \frac{\dot{M}fg^{-1}}{3\pi}\left(1 - \frac{l^2p}{p+\frac{1}{2}}\right), \tag{18}$$

where $g = -(2/3)(d\ln\Omega_{\rm K}/d\ln R)$ and the factor $f = 1 - [\Omega(3R_g)/\Omega(R)](3R_g/R)^{p+2}$.

In line with prior work, we employ self-similar assumptions and adopt $\gamma = 1.5$. (e.g., R. Narayan & I. Yi 1994; W.-M. Gu & J.-F. Lu 2000). Under these assumptions, Equations (10), and (13)–(14) reduce to the following forms:

$$\frac{1}{2}V_R^2 + \frac{5}{2}(c_g^2 + c_r^2) + c_g\Omega_K R - c_g R^2\frac{d\Omega_K}{dR} + \left(\Omega^2 - \Omega_{\rm K}^2\right)R^2 = 0, \tag{19}$$

$$Q_{\rm vis} = \frac{3\dot{M}\Omega^2fg}{4\pi}\left(1 - \frac{l^2p}{p+\frac{1}{2}}\right), \tag{20}$$

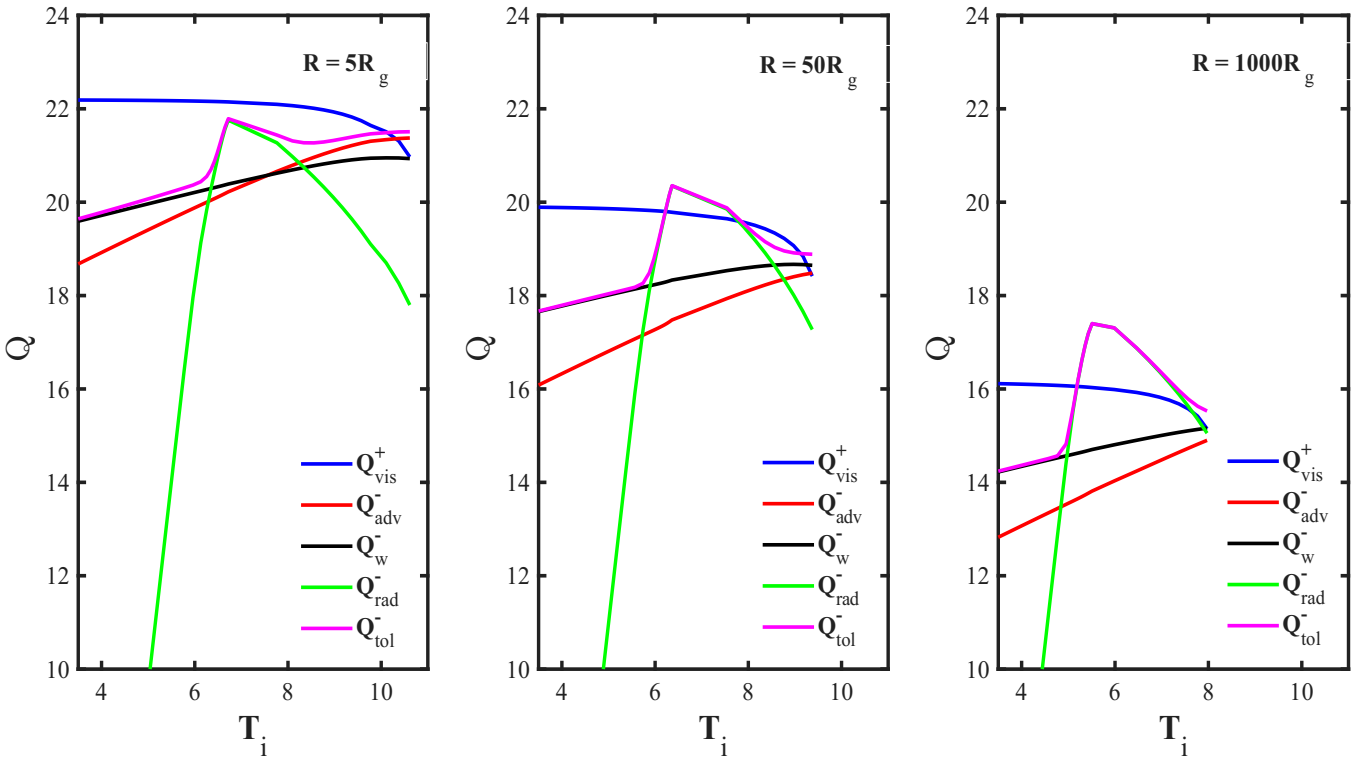

Figure 2. The figure presents the variation of heating and cooling rates with T_i. Here, $Q^{+}_{\rm vis}$ is the total heating rate, while $Q^{-}_{\rm adv}$, Q^{-}_{w}, $Q^{-}_{\rm rad}$, and $Q^{-}_{\rm tot}$ represent the advective, outflow, radiative, and total cooling rates, respectively.

$$Q_{\rm adv} = \frac{1}{4\pi}\frac{\dot{M}}{R^2}(c_g^2 + c_r^2 - 5V_A^2) - \left(\frac{\dot{M}c_g}{\pi}\frac{d\Omega_K}{dR}\right), \qquad (21)$$

where $c_r = \sqrt{P_{\rm rad}/\rho}$.

Finally, substituting Equation (9) into Equation (17) yields

$$Q_w = \frac{f\eta p\dot{M}\Omega_K^2}{2\pi}. \qquad (22)$$

By solving the five equations—Equations (1), (8), (12), and (18)–(19)—for the five variables ρ, T_i, c_s, Ω, and V_R with the given parameters $M_{\rm BH}$, α, $\dot{M}$, λ, η, ξ, and l, we obtain the thermal equilibrium solutions of accretion flows.

3. Numerical Results

In this section, we discuss the effects of magnetic fields on accretion disks. Figure 1 illustrates how the relative magnetic field strength influences the thermal equilibrium solution of the accretion disk. Here, $M_{\rm BH} = 10M_{\odot}$, $\alpha = 0.1$, $l = 1$, $\eta = 1$, $\dot{m} \equiv \dot{M}/\dot{M}_{\rm Edd}$, where $\dot{M}_{\rm Edd} = 64\pi GM_{\rm BH}/c\kappa_{\rm es}$ is the Eddington accretion rate. For $\xi = 0$, there exist five types of solutions similar to those described in X. Chen et al. (1995): the ADAF and SLE solutions on the left branch, the slim disk solutions, as well as the unstable SSD and the stable SSD solutions on the right branch. It can be seen from the figure that as the magnetic field strengthens, the topological morphology of the thermal equilibrium solution of the accretion disk changes. For $R = 5R_{\rm g}$, when $\xi = 1$, meaning the magnetic field is fully saturated, a new thermal equilibrium solution emerges. At this point, the optically thick radiative cooling (similar to the SSD) solution completely vanishes, leaving only the advection-dominated solutions (similar to ADAF and slim solutions). For $R = 50R_{\rm g}$, when $\xi = 1$, the topological structure also differs from the conventional form. Not only does the unstable optically thick radiative cooling solution vanish, but the optically thin solutions connected to the optically thick solutions. Furthermore, for the saturated state at $R = 50R_{\rm g}$, we find that the critical value for the existence of optically thin advection-dominated solutions is larger than that without magnetic pressure. This finding may provide an explanation for the hard X-ray behavior observed during state transitions (N. Scepi et al. 2024). In addition, the optically thick radiative cooling solution appears to exhibit a lower limit.

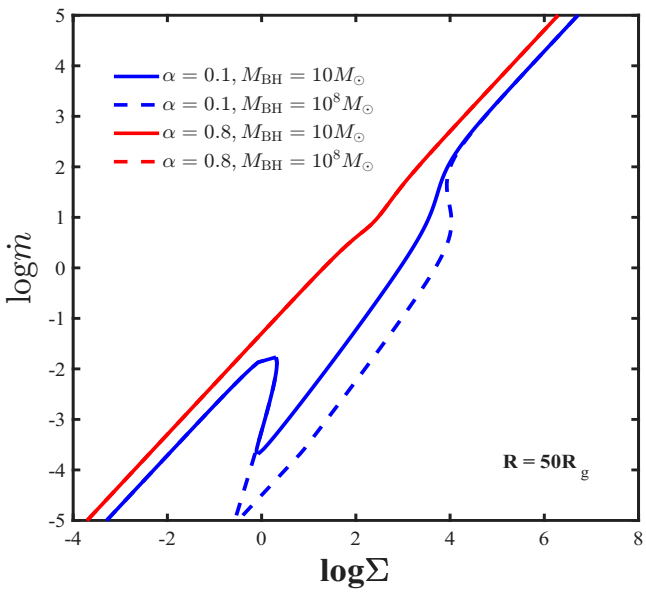

Figure 3. Thermal equilibrium solutions are plotted for different α and $M_{\rm BH}$ at $R = 50R_g$. Blue and red curves represent cases with $\alpha = 0.1$ and $\alpha = 0.8$, respectively. In the figure, the solid and dashed red lines coincide.

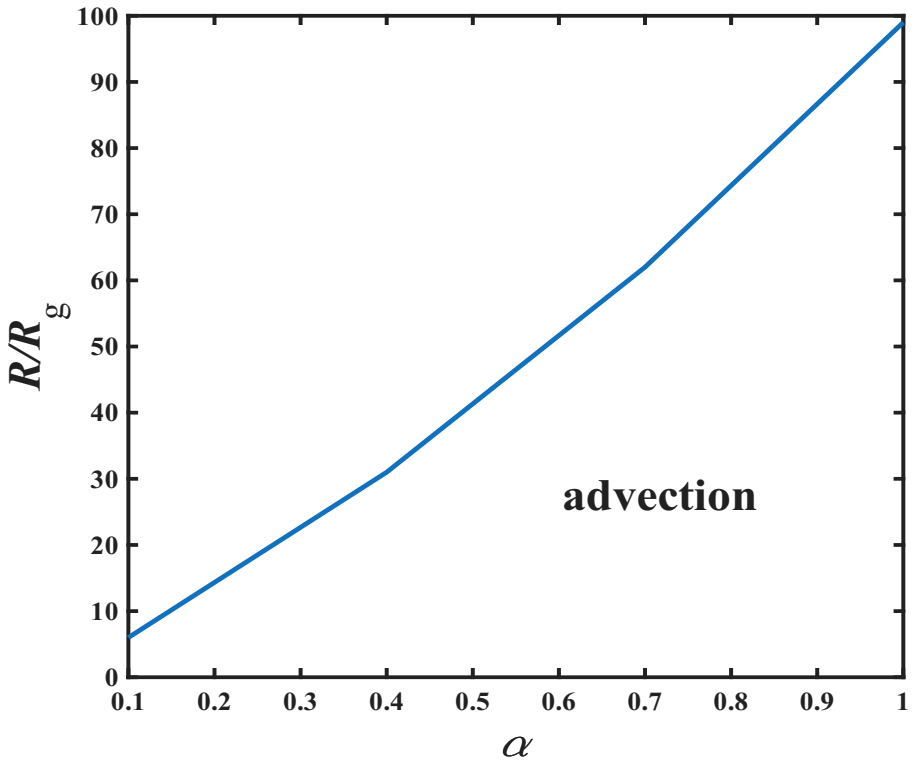

Figure 4. The radial distribution of the advection solution as a function of α for $\xi = 1$ is shown in the figure.

To understand the differences in topological structure at small and large radii, particularly that the optically thick radiative cooling solution disappears at small radii, Figure 2 provides a qualitative explanation ($\xi = 1$). We assume $\dot{m} = 0.01$ at $R = 10R_g$, and solve for the variation of heating and cooling rates with T_i at different radii ($R = 5R_g$, $R = 50R_g$, $R = 1000R_g$), where the condition for establishing the thermal equilibrium solution is $Q^+_{\rm vis} = Q^-_{\rm tot} (= Q^-_{\rm adv} + Q^-_{\rm w} + Q^-_{\rm rad})$. At $R = 5R_g$, the thermal equilibrium solution resides at $T_{\rm i} \sim 10^{10} K$, where radiative cooling becomes almost negligible. This indicates the absence of optically thick radiative cooling solutions at small radii, with advective cooling dominating the energy balance. At $R = 50R_g$, three distinct solutions coexist: the low-temperature, optically thick radiative cooling solution; the optically thin radiative cooling solution (similar to the SLE); and the high-temperature, optically thin advective cooling solution. This configuration suggests possible coexistence between optically thick radiative cooling solutions and optically thin advective cooling solutions at this radius. At $R = 1000R_g$, however, only the optically thick radiative cooling solution exists (see also J. Huang et al. 2023).

X. Chen et al. (1995) discovered that for $\alpha > \alpha_{\rm crit}$, the thermal equilibrium solutions of accretion flows exhibit a novel topological structure. In this regime, we compute the thermal equilibrium solutions for accretion flows at $\alpha = 0.8$. For the saturated state, the solution at $R = 5R_{\rm g}$ remains unchanged. However, at $R = 50R_g$, a novel topological structure emerges: the original optically thick radiative cooling solution vanishes, while the optically thick and optically thin advection-dominated solutions become connected. This configuration is consistent with the topological structure observed at $R = 5R_g$, as illustrated in Figure 3. For optically thick, radiative-cooling disks with $\xi = 1$, we have $V_A \gg c_g$. By following the derivation in the appendix of W.-B. Wu & W.-M. Gu (2023), we obtain

$$V_R = -\frac{3}{2}\frac{\alpha f^{-1} g}{R}\left(1 - \frac{l^2 p}{p + 1/2}\right)^{-1} c_g, \tag{23}$$

$$\frac{H}{R} = 8.1 \times 10^{-2} (\alpha m)^{-1/18} \dot{m}^{1/9} x^{-13/36} (x - 1)^{7/18} \times \left[3g\left(1 - \frac{l^2 p}{p + 1/2}\right)^2 - 2\eta p\left(1 - \frac{l^2 p}{p + 1/2}\right)\right]^{1/18} \times f^{1/9} g^{-1/18}, \tag{24}$$

$$\frac{H_{\rm SSD}}{R} = 1.2 \times 10^{-2} (\alpha m)^{-1/10} \dot{m}^{1/5} x^{-13/20} (x - 1)^{7/10} f^{1/5}, \tag{25}$$

where $x \equiv R/R_g$ and $m = M_{\rm BH}/(10M_\odot)$. Equation (23) implies that an increase in α enhances the radial velocity, thereby leading to an expansion of the advection-dominated domain (where $Q^-_{\rm adv} \gg Q^-_{\rm rad}$). Figure 4 shows the dependence of this advection-dominated regime on α.

Theoretical (e.g., N. I. Shakura & R. A. Sunyaev 1973) and numerical simulations (e.g., Y.-F. Jiang et al. 2019) indicate that radiation pressure plays a more significant role in accretion disks around supermassive black holes compared to those around stellar-mass black holes. To investigate the impact of radiation pressure in both cases, we computed the thermal equilibrium solutions at $R = 5R_g$ and $R = 50R_g$ under the condition of $\alpha = 0.1$ for $M = 10M_\odot$ and $M = 10^8 M_\odot$, as shown in Figure 5. At $R = 5R_g$ under the saturated state, only advection-dominated solutions exist for supermassive black hole accretion systems, showing no discernible difference in radiation pressure effects. However, at $R = 50R_g$, the lower existence limit for optically thick radiative cooling solutions becomes reduced. More significantly, unlike stellar-mass black

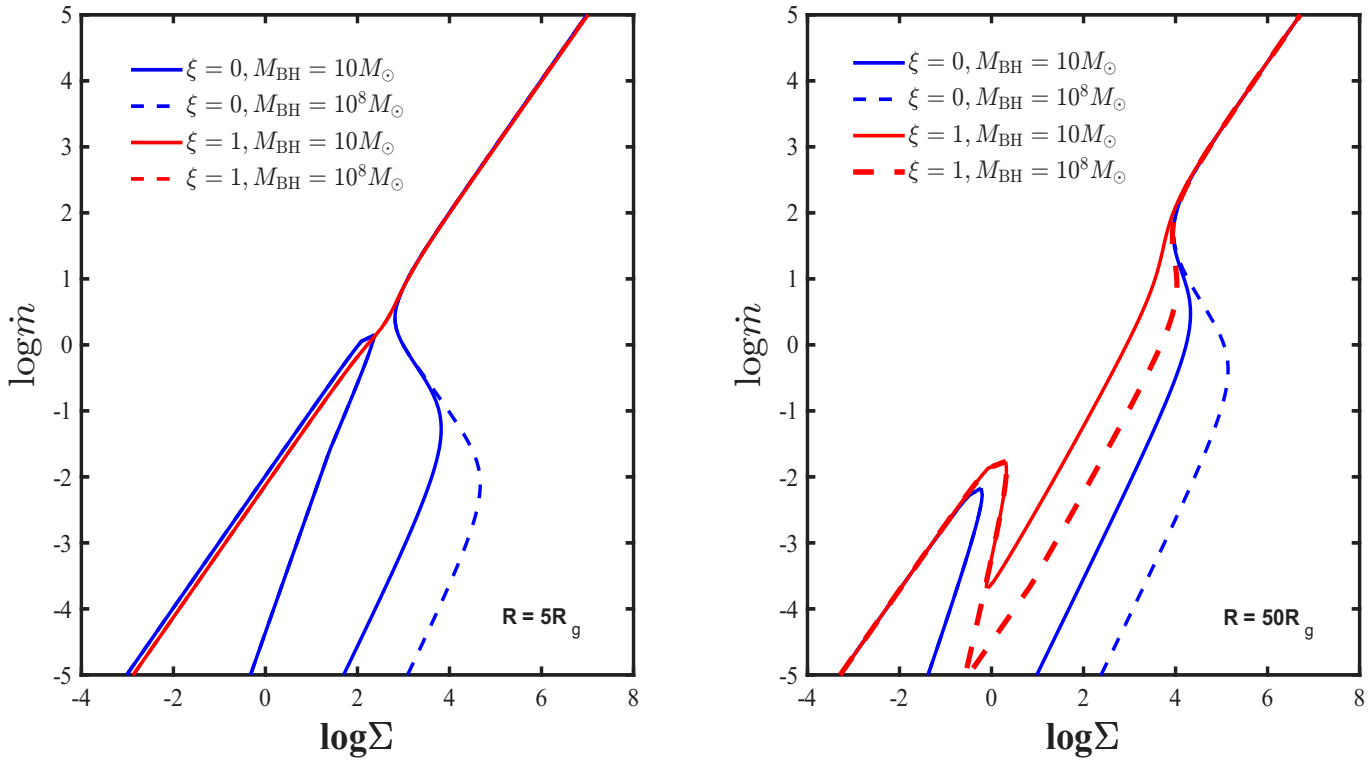

Figure 5. For $\alpha = 0.1$, thermal equilibrium solutions for different black hole masses are presented in the left ($\xi = 0$) and right ($\xi = 1$) panels. In the left panel, the solid and dashed red lines coincide.

hole accretion systems, which exhibit only stable optically thick radiative cooling solutions, supermassive black hole accretion systems now present both stable and unstable branches—though the parameter space for unstable solutions remains smaller compared to the $\xi = 0$ case. Additionally, a comparison of Equations (24) and (25) shows that $H_{\rm SSD}/R \sim (H/R)^{1.8}$, indicating that the scale height of the optically thick radiative cooling flow ($\xi = 1$) is approximately 1 order of magnitude larger than that of the SSD model. Moreover, for the optically thick radiative cooling flow ($\xi = 1$), we obtain $H/R \sim 0.1$ for $M = 10M_\odot$ and $H/R \sim 0.03$ for $M = 10^8M_\odot$. These results suggest that advection plays a more significant role in accretion disks around stellar-mass black holes than in those around supermassive black holes, effectively transporting energy generated by viscosity without accumulation that could lead to instabilities.

Figure 6 shows the thermal equilibrium solutions for different black hole masses. From the figure, we observe that when $M \geqslant 10^5M_\odot$, unstable optically thick radiative cooling solutions become increasingly pronounced, indicating that radiation pressure begins to exert a significant influence. The SSD model suggests that radiation pressure dominance would lead to dramatic variability in accretion disks for both XRBs and AGNs. However, there is a lack of supporting observational evidence for this prediction in XRBs. According to our results, for stellar-mass black hole accretion systems, the dominance of magnetic pressure over radiation pressure suppresses such instabilities, thereby explaining the absence of strong variability in observations. In this regime, only stable optically thick radiative cooling solutions exist. An exception is a class of variability phenomena termed "heartbeat" oscillations observed in XRBs (e.g., J. Neilsen et al. 2011), which may be attributed to radiation pressure instability (e.g., Q. Wu et al. 2016). Additionally,

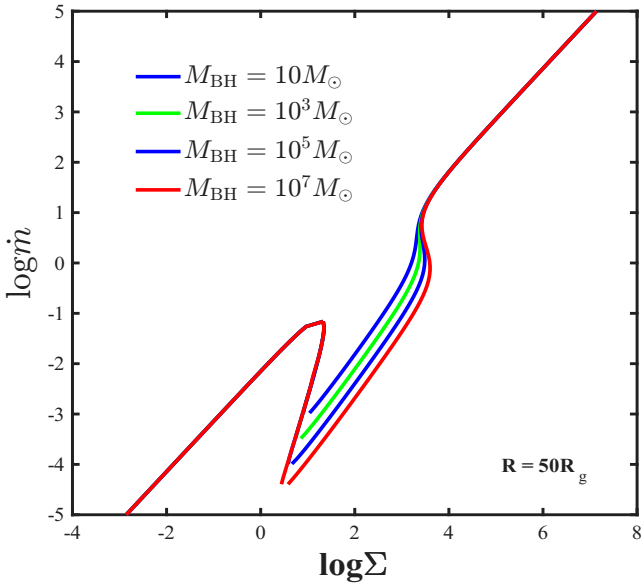

Figure 6. The figure shows thermal equilibrium solutions for different black hole masses at $\xi = 1$, $\alpha = 0.1$, and $R = 50R_g$.

numerical simulations suggest that whether an accretion disk can reach the saturated state may depend on the initial ratio of vertical magnetic field strength to equatorial gas pressure (e.g., X.-N. Bai & J. M. Stone 2013; G. Salvesen et al. 2016). Therefore, for cases with $\xi < 1$ in Figure 1, unstable optically thick radiative cooling solutions may emerge. Nevertheless, recent observations have identified a class of variability known as quasiperiodic eruptions (QPEs)—a phenomenon with no analogous counterpart observed in XRBs (e.g., G. Miniutti et al. 2019; M. Giustini et al. 2020; R. Arcodia et al. 2021). This

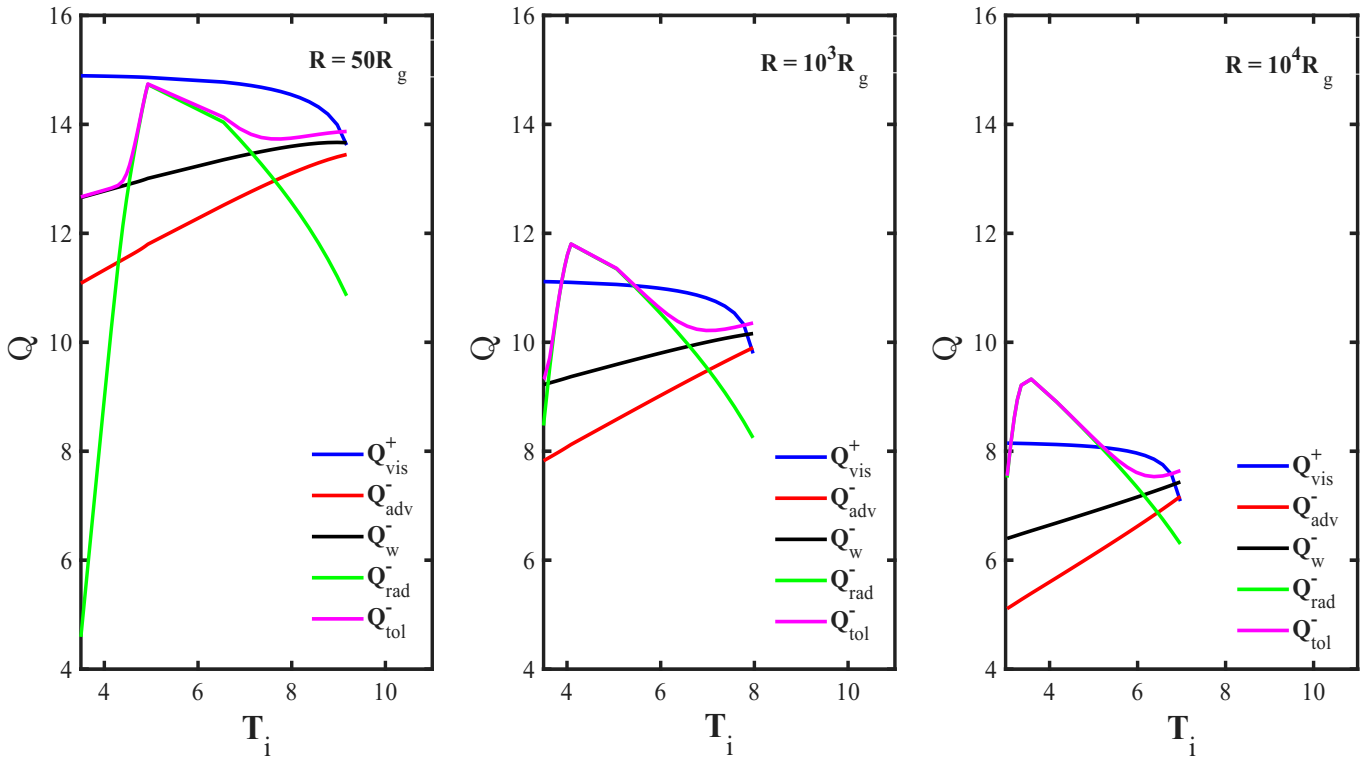

Figure 7. The figure shows the variation of heating and cooling rates with T_i for $M = 10^6 M_\odot$ and $\alpha = 0.8$. All quantities have the same definitions as in Figure 2.

notable absence supports our theoretical proposal that radiation pressure plays, specifically, an increasingly critical role in supermassive black hole accretion systems. Thus, magnetically dominated accretion disks ($\xi = 1$) offer a plausible explanation for the observed discrepancies between the SSD model and observations. Recently, related work has begun exploring this issue (K. Kaur et al. 2023).

4. Conclusions and Discussion

This study extends our previous work by investigating the thermal equilibrium solutions for $\alpha > \alpha_{\rm crit}$ and their effects on different black hole accretion systems. We find that when the disk becomes magnetically dominated ($\xi = 1$), the inner region is dominated by advection-dominated solutions (where $Q_{\rm adv}^- \gg Q_{\rm rad}^-$), whereas optically thick radiative cooling solutions cease to exist. This occurs because in the inner disk region, radiative cooling becomes negligible compared to viscous heating. For $\alpha > \alpha_{\rm crit}$, a distinct topological structure emerges at large radii, accompanied by a radial expansion of the advection-dominated region. Moreover, in magnetically dominated accretion disks around stellar-mass black holes, the magnetic pressure significantly exceeds radiation pressure, thereby suppressing instabilities and thus explaining the absence of observed strong variability in XRBs. Conversely, in the case of supermassive black hole accretion systems, radiation pressure regains significance, thereby providing an explanation for the QPEs observed in recent years (e.g., G. Miniutti et al. 2019; M. Giustini et al. 2020; R. Arcodia et al. 2021). Furthermore, numerous studies have found that magnetically dominated accretion disks also offer a compelling explanation for changing-look AGNs (e.g., J. Dexter & M. C. Begelman 2019; J. Feng et al. 2021; N. Scepi et al. 2021; W.-B. Wu & W.-M. Gu 2023).

Table 1
Transition Radii for Binary Systems and AGNs (Data from F. Yuan & R. Narayan 2014 and Citations Therein)

Name	$R_{\rm tr}(R/R_g)$
M81	100
NGC 4579	100
NGC 5548	30–80
XTE J1118+480	300
NGC 1097	225
XBONG: "Source #1"	60
M87	10^4
Sgr A^*	10^4

The observed energy spectra often cannot be explained by a single disk component, as exemplified by the hard state in XRBs. Such cases are typically modeled using a combined SSD+ADAF configuration (e.g., R. Narayan et al. 1998; R. Narayan & J. E. McClintock 2008), where the ADAF accounts for the harder spectral component, while the SSD explains the blackbody-like spectrum. This, however, raises a fundamental question: how are the SSD and ADAF connected? According to the strong ADAF principle (R. Narayan & I. Yi 1995), when both flows are theoretically possible, the ADAF solution is favored over the SSD. Based on the findings presented in this work, we propose a new interpretation: although structurally similar to an SSD, a magnetically dominated accretion disk has a scale height roughly 1 order of magnitude larger than that of an SSD. Consequently, the radial velocity of the accretion flow becomes significantly larger than that in an SSD (as shown in Equations (24) and (25)). As the flow moves inward, the larger scale height and radial velocity reduce the optical depth through a substantial drop in density, making advection increasingly significant and culminating in a transition to an ADAF. Table 1 compiles the transition radii for

several binary systems and AGNs (F. Yuan & R. Narayan 2014). With the exception of M87 and Sgr A^*, the other sources listed in Table 1 show reasonably good agreement with the results obtained in this study. Indeed, Figure 4 shows the advection-dominated regions; outside these regions, there exists a coexistence region where both SSD and ADAF solutions are possible, as illustrated at $50R_g$ for $\alpha = 0.1$ in Figure 2. Regarding M87 and Sgr A^*, although their transition radii are observed at 10^4R_g, such large transition radii remain theoretically possible even for $\alpha > \alpha_{\rm crit}$. Figure 7 presents results for $M = 10^6M_\odot$ with $\alpha = 0.8$. Our calculations reveal that at $\alpha = 0.8$ and a radius of 10^4R_g, SSD and ADAF solutions can coexist, suggesting that the transition radius may indeed extend to 10^4R_g. We emphasize that the solutions in this work are derived under the self-similar assumption and therefore provide qualitative interpretations; in subsequent work, we will pursue global solutions following approaches like that of J.-F. Lu et al. (2004), directly solving the differential equations with boundary and sonic point conditions to obtain quantitative transition radii and check our results.

Acknowledgments

The author thanks Wei-Min Gu for insightful discussions and the anonymous referee for constructive suggestions that improved the paper. This work was supported by the Doctoral Scientific Research Start-up Foundation of Nanchang Normal University (grant No. NSBSJJ2024005).

References

Abramowicz, M. A. 1981, Natur, 294, 235
Abramowicz, M. A., Chen, X., Kato, S., et al. 1995, ApJL, 438, L37
Abramowicz, M. A., Chen, X.-M., Granath, M., et al. 1996, ApJ, 471, 762
Abramowicz, M. A., Czerny, B., Lasota, J. P., et al. 1988, ApJ, 332, 646
Arcodia, R., Merloni, A., Nandra, K., et al. 2021, Natur, 592, 704
Blandford, R. D., & Begelman, M. C. 1999, MNRAS, 303, L1
Blandford, R. D., & Payne, D. G. 1982, MNRAS, 199, 883
Balbus, S. A., & Hawley, J. F. 1991, ApJ, 376, 214
Begelman, M. C., Armitage, P. J., & Reynolds, C. S. 2015, ApJ, 809, 118
Begelman, M. C., & Pringle, J. E. 2007, MNRAS, 375, 1070
Bai, X.-N., & Stone, J. M. 2013, ApJ, 769, 76
Cao, X., & Gu, W.-M. 2015, MNRAS, 448, 3514
Cao, X., & Gu, W.-M. 2022, ApJ, 936, 141
Cao, X., & Spruit, H. C. 2013, ApJ, 765, 149
Chen, X., Abramowicz, M. A., Lasota, J.-P., et al. 1995, ApJL, 443, L61
Dexter, J., & Begelman, M. C. 2019, MNRAS, 483, L17
Feng, J., Cao, X., Gu, W.-M., et al. 2019, ApJ, 885, 93
Feng, J., Cao, X., Li, J.-. wen, et al. 2021, ApJ, 916, 61
Gu, W.-M. 2015, ApJ, 799, 71
Gu, W.-M., & Lu, J.-F. 2000, ApJL, 540, L33
Gu, W.-M., & Lu, J.-F. 2007, ApJ, 660, 541
Giustini, M., Miniutti, G., & Saxton, R. D. 2020, A&A, 636, L2
Homan, J., Neilsen, J., Allen, J. L., et al. 2016, ApJL, 830, L5
Habibi, A., & Abbassi, S. 2019, ApJ, 887, 256
Huang, J., Feng, H., Gu, W.-M., et al. 2023, ApJ, 954, 150
Huang, J., Feng, H., & Tao, L. 2025, ApJ, 985, 217
Huang, J., Jiang, Y.-F., Feng, H., et al. 2023, ApJ, 945, 57
Igumenshchev, I. V., Narayan, R., & Abramowicz, M. A. 2003, ApJ, 592, 1042
Jiang, Y.-F., Blaes, O., Stone, J. M., et al. 2019, ApJ, 885, 144
Jiang, Y.-F., Stone, J. M., & Davis, S. W. 2014, ApJ, 796, 106
Jacquemin-Ide, J., Ferreira, J., & Lesur, G. 2019, MNRAS, 490, 3112
Kato, S., Fukue, J., & Mineshige, S. 2008, Black-Hole Accretion Disks—Towards a New Paradigm (Kyoto Univ. Press)
Kitaki, T., Mineshige, S., Ohsuga, K., et al. 2017, PASJ, 69, 92
Kitaki, T., Mineshige, S., Ohsuga, K., et al. 2018, PASJ, 70, 108
Knigge, C. 1999, MNRAS, 309, 409
Kaur, K., Stone, N. C., & Gilbaum, S. 2023, MNRAS, 524, 1269
Lu, J.-F., Lin, Y.-Q., & Gu, W.-M. 2004, ApJL, 602, L37
Miniutti, G., Saxton, R. D., Giustini, M., et al. 2019, Natur, 573, 381
Ma, R.-Y., Roberts, S. R., Li, Y.-P., et al. 2019, MNRAS, 483, 5614
Narayan, R., & Yi, I. 1994, ApJL, 428, L13
Narayan, R., & Yi, I. 1995, ApJ, 444, 231
Narayan, R., & Yi, I. 1995, ApJ, 452, 710
Narayan, R., Mahadevan, R., & Quataert, E. 1998, Theory of Black Hole Accretion Disks (Cambridge Univ. Press), 148
Narayan, R., & McClintock, J. E. 2008, NewAR, 51, 733
Narayan, R., Sądowski, A., Penna, R. F., et al. 2012, MNRAS, 426, 3241
Neilsen, J., Remillard, R. A., & Lee, J. C. 2011, ApJ, 737, 69
Nomura, M., Ohsuga, K., & Done, C. 2020, MNRAS, 494, 3616
Nomura, M., Ohsuga, K., Takahashi, H. R., et al. 2016, PASJ, 68, 16
Oda, H., Machida, M., Nakamura, K. E., et al. 2009, ApJ, 697, 16
Ohsuga, K., & Mineshige, S. 2011, ApJ, 736, 2
Ohsuga, K., Mori, M., Nakamoto, T., et al. 2005, ApJ, 628, 368
Piran, T. 1978, ApJ, 221, 652
Paczyński, B., & Wiita, P. J. 1980, A&A, 88, 23
Pessah, M. E., & Psaltis, D. 2005, ApJ, 628, 879
Park, J., Hada, K., Kino, M., et al. 2019, ApJ, 871, 257
Shapiro, S. L., Lightman, A. P., & Eardley, D. M. 1976, ApJ, 204, 187
Sadowski, A. 2016, MNRAS, 459, 4397
Sadowski, A., & Narayan, R. 2015, MNRAS, 453, 3213
Sadowski, A., Narayan, R., McKinney, J. C., et al. 2014, MNRAS, 439, 503
Shakura, N. I., & Sunyaev, R. A. 1973, A&A, 24, 337
Stone, J. M., Pringle, J. E., & Begelman, M. C. 1999, MNRAS, 310, 1002
Salvesen, G., Simon, J. B., Armitage, P. J., et al. 2016, MNRAS, 457, 857
Scepi, N., Begelman, M. C., & Dexter, J. 2021, MNRAS, 502, L50
Scepi, N., Dexter, J., Begelman, M. C., et al. 2024, A&A, 692, A153
Shi, F., Li, Z., Yuan, F., et al. 2021, NatAs, 5, 928
Wu, Q., Czerny, B., Grzedzielski, M., et al. 2016, ApJ, 833, 79
Wu, W.-B., & Gu, W.-M. 2023, ApJ, 958, 146
Wu, W.-B., Gu, W.-M., & Sun, M. 2022, ApJ, 930, 108
Wang, Q. D., Nowak, M. A., Markoff, S. B., et al. 2013, Sci, 341, 981
Yuan, F., Bu, D., & Wu, M. 2012a, ApJ, 761, 130
Yuan, F., Gan, Z., Narayan, R., et al. 2015, ApJ, 804, 101
Yuan, F., & Narayan, R. 2014, ARA&A, 52, 529
Yuan, F., Wu, M., & Bu, D. 2012b, ApJ, 761, 129
Yu, X.-F., Gu, W.-M., Liu, T., et al. 2015, ApJ, 801, 47
Zahra Zeraatgari, F., Mosallanezhad, A., Yuan, Y.-F., et al. 2020, ApJ, 888, 86
Zheng, S.-M., Yuan, F., Gu, W.-M., et al. 2011, ApJ, 732, 52